JACS
JOURNAL OF THE AMERICAN CHEMICAL SOCIETY
Article
Cite This: J. Am. Chem. Soc. 2018, 140, 4678−4683
pubs.acs.org/JACS

Chemical Pressure-Driven Enhancement of the Hydrogen Evolving Activity of Ni_2P from Nonmetal Surface Doping Interpreted via Machine Learning

Robert B. Wexler,[†] John Mark P. Martirez,[‡] and Andrew M. Rappe*[,†]

[†]Department of Chemistry, University of Pennsylvania, Philadelphia, Pennsylvania 19104-6323, United States
[‡]Department of Mechanical and Aerospace Engineering, Princeton University, Princeton, New Jersey 08544, United States

Supporting Information

ABSTRACT: The activity of Ni_2P catalysts for the hydrogen evolution reaction (HER) is currently limited by strong H adsorption at the Ni_3-hollow site. We investigate the effect of surface nonmetal doping on the HER activity of the Ni_3P_2 termination of $Ni_2P(0001)$, which is stable at modest electrochemical conditions. Using density functional theory (DFT) calculations, we find that both 2*p* nonmetals and heavier chalcogens provide nearly thermoneutral H adsorption at moderate surface doping concentrations. We also find, however, that only chalcogen substitution for surface P is exergonic. For intermediate surface concentrations of S, the free energy of H adsorption at the Ni_3-hollow site is −0.11 eV, which is significantly more thermoneutral than the undoped surface (−0.45 eV). We use the regularized random forest machine learning algorithm to discover the relative importance of structure and charge descriptors, extracted from the DFT calculations, in determining the HER activity of $Ni_2P(0001)$ under different doping concentrations. We discover that the Ni−Ni bond length is the most important descriptor of HER activity, which suggests that the nonmetal dopants induce a chemical pressure-like effect on the Ni_3-hollow site, changing its reactivity through compression and expansion.

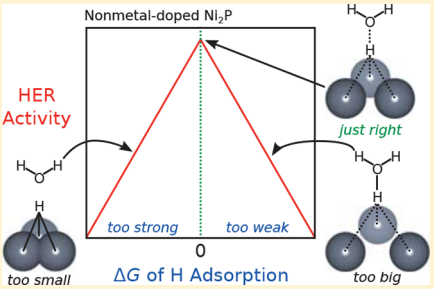

INTRODUCTION

The discovery of highly active, noble-metal-free catalysts for the hydrogen evolution reaction (HER) is crucial for the development of economical water-splitting fuel storage technologies. There have been many candidates proposed in the past two decades, most notably MoS_2[1,2] and Ni_2P.[3,4] Recently, we found that the bulk-like Ni_3P_2 termination of the $Ni_2P(0001)$ surface, which is stable at modest electrochemical conditions, i.e., reducing potentials greater than −0.21 V vs the standard hydrogen electrode (SHE) and pH = 0, is not catalytically active because the Ni_3-hollow site binds H too strongly (ΔG_H = −0.45 eV).[5] Upon the application of −0.21 V vs SHE, however, the surface becomes enriched with P adatoms, which provide nearly thermoneutral H adsorption and consequently catalytic activity toward the HER.[5]

In order to overcome the inactivity of the Ni_3-hollow site, attempts have been made to tune the HER activity of Ni_2P by doping with different transition metals such as Co,[6−8] Fe,[9] Mn,[10] and Mo.[11] There have been no attempts, however, to dope Ni_2P with nonmetals, despite the host of stable binary Ni-nonmetal compounds that exist in nature and are catalytically active toward water splitting such as Ni_3N,[12] Ni_3Se_2,[13] and Ni_3C.[14] Furthermore, there have been no studies, experimental or theoretical, that investigate the effect of surface doping on the HER activity of Ni_2P, as most studies have considered bulk doping. Here, we study the influence of surface nonmetal doping on the surface structure, charge states, and HER activity of $Ni_2P(0001)$ using density functional theory (DFT) calculations. We find that the Ni−Ni bond length is a robust descriptor for the HER activity of $Ni_2P(0001)$ using machine learning based on regularized random forests.[15] This paper outlines a transferable approach for the use of machine learning to extract descriptors from DFT structural and charge data.

METHODS

First-Principles Calculations. Spin-polarized DFT calculations were performed using the Quantum Espresso code (version 5.1).[16] Optimized, norm-conserving, designed nonlocal pseudopotentials were used to replace the nuclear Coulomb potential plus core electrons with a smoother, effective potential.[17,18] The valence electron wave functions were expanded in a plane-wave basis with an energy cutoff of 50 Ry. The generalized gradient approximation (GGA) of Perdew, Burke, and Ernzerhof (PBE)[19] was used to calculate the exchange-correlation energy. Grimme's semiempirical DFT-D2 method[20,21] was used to include dispersion interactions, which are generally important for accurately modeling catalytic processes.[22,23] We choose the DFT-D2 method because it shows excellent agreement with higher-level electron correlation methods, i.e., Møller−Plesset perturbation theory (MP2) and coupled-cluster singles and doubles (CCSD), for H adsorption energies.[24,25]

We modeled the HER on an eight-layer, periodic slab of Ni_2P. The dimensions of the slab were $a = b$ = 10.07 Å and c = 39.57 Å, and $\alpha = \beta = 90°$ and $\gamma = 120.08°$. The width of the vacuum region was 26.24 Å.

Received: January 24, 2018
Published: March 19, 2018

DOI: 10.1021/jacs.8b00947
J. Am. Chem. Soc. 2018, 140, 4678−4683

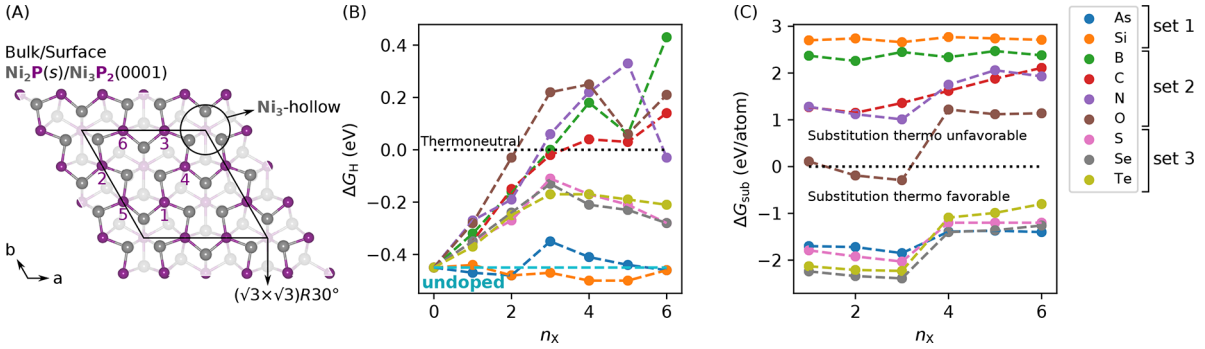

Figure 1. (A) Structure of $Ni_3P_2(0001)$ surface of Ni_2P showing the $(\sqrt{3} \times \sqrt{3})R30°$ supercell. The Ni_3-hollow sites, which bind H, are shown. The indices on P atoms indicate the preferred sequence of substitution with dopants. Free energy of (B) H adsorption and (C) dopant substitution as a function of the surface dopant concentration. $\Delta G_H = 0$ is referred to as "thermoneutral" H adsorption. ΔG_H for the undoped surface is labeled and denoted by a dashed, light blue line. The spontaneity of dopant substitution is labeled and indicated by a dotted black line.

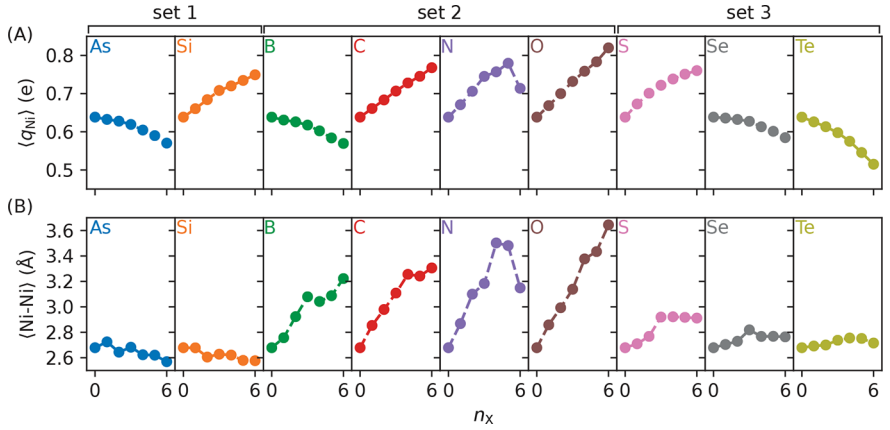

Figure 2. Effect of dopant and surface concentration on the (A) average Ni residual charge ($\langle q_{Ni} \rangle$) and (B) average Ni−Ni bond length ($\langle$Ni−Ni$\rangle$).

A $(\sqrt{3} \times \sqrt{3})R30°$ surface supercell was used so that we could model fractional surface concentrations of nonmetal dopants. A Γ-centered, 3 × 3 × 1 grid of *k*-points was used to sample the Brillouin zone. During geometry relaxations, the bottom four layers of the slab were fixed in their bulk configurations.

Machine Learning. Regularized random forests (RRFs) were trained using the caret package (version 6.0.77) for R (version 3.2.5).[26] Processed data and R scripts for the machine learning can be found in the Supporting Information. 3-fold cross-validation (CV) was performed to improve our prediction of the "out-of-sample" error. At each step of the training process, 10 descriptors were randomly selected and a regularization value of 0.1 and an importance coefficient of 0.75 were applied. More details on the DFT calculations and machine learning can be found in the Supporting Information.

RESULTS AND DISCUSSION

Surface Structure and Doping Scheme. Bulk $Ni_2P(s)$ has two alternating layers along the [0001] axis with compositions of Ni_3P and Ni_3P_2. Figure 1A shows the structure of the $Ni_3P_2(0001)$ termination. The surface has one Ni_3-hollow site per unit cell (three per $\sqrt{3} \times \sqrt{3}R30°$ supercell). In an aqueous electrochemical environment at $U = 0$ V vs SHE and pH = 0, each Ni_3-hollow site binds H strongly ($\Delta G_H = -0.45$ eV, $n_X = 0$ in Figure 1B). Each Ni bonds with two P in the surface layer and one P in the subsurface layer. This makes for a total of six symmetry-equivalent P atoms surrounding the Ni_3-hollow site in the surface layer, which are numbered from 1 through 6 in Figure 1A. We replace these surface P sites with nine different nonmetals (As, B, C, N, O, S, Se, Si, and Te) and varied the number of dopants (n_X) from 1 to 6. We found that the S dopants prefer being separated at $n_S = 2$, i.e., S at positions 1 and 2 is more favorable than when they are sharing a common Ni (at positions 1 and 5) by 0.34 eV. Thus, for other dopants, and at higher doping concentrations, the maximum separation between dopants is maintained. The indices on P in Figure 1A correspond to the preferred sequence of substitution of the P atoms. For example, at $n_X = 3$, dopants are substituted at sites 1, 2, and 3. While the Ni and P sites are symmetrically equivalent initially, doping breaks this symmetry.

Effect of Doping Concentration on H Adsorption and Dopant Substitution. *H Adsorption.* The effect of surface dopant identity and concentration on ΔG_H at the Ni_3-hollow site is shown in Figure 1B. We observe three distinct trends corresponding to (1) As and Si, (2) 2*p* nonmetals (B, C, N, and O), and (3) chalcogenides (S, Se, and Te). The first set does not differ appreciably from the undoped surface (dashed, light blue line marked "undoped"). ΔG_H is relatively constant with respect to changes in the surface dopant concentration. Conversely, 2*p* nonmetals (set 2) have a dramatic effect on ΔG_H, which generally increases with increasing n_X. Nearly thermoneutral H adsorption is possible for $n_X = 2$–3 (50% substitution) and, above that, H adsorption is no longer favored. The chalcogenides (set 3), on the other hand, have an intermediate effect on ΔG_H. From $n_X = 1$ to 3, ΔG_H increases at about the same rate for each chalcogenide. From $n_X = 4$ to 6, however, ΔG_H decreases, with the attenuation being more pronounced for S and Se than Te. The maximum ΔG_H achieved is −0.11 eV for S at $n_X = 3$. Therefore, doping the

DOI: 10.1021/jacs.8b00947
J. Am. Chem. Soc. 2018, 140, 4678−4683

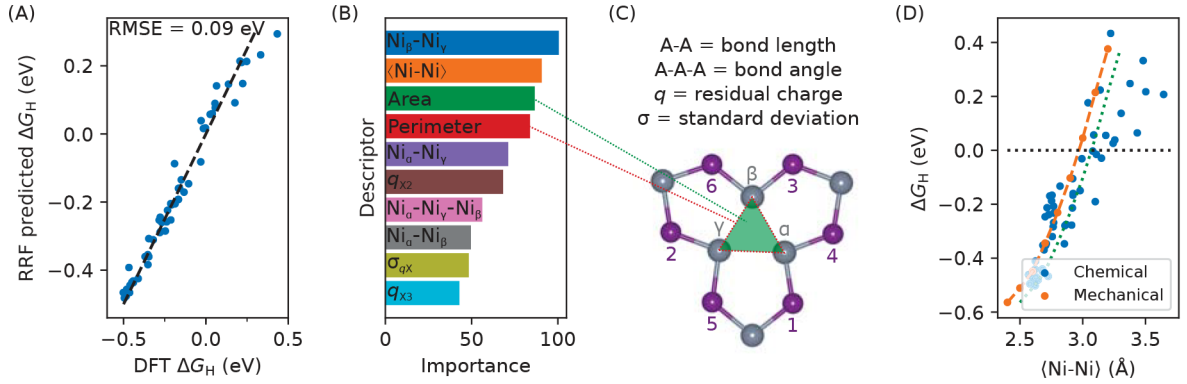

Figure 3. (A) ΔG_H predicted by RRFs vs DFT. Black-dashed line corresponds to perfect agreement. (B) Relative importance of descriptors calculated from RRF model. Only the top 10 features are shown (see Figure S2 in the Supporting Information for full list). (C) Definition of descriptors in (B). We label the three Ni atoms α, β, and γ based on their distance from the first doping site. (D) Effect of average Ni−Ni bond length on ΔG_H as induced by chemical pressure and mechanical pressure. Chemical pressure was induced by surface nonmetal doping and mechanical pressure by fixing the positions of surface Ni atoms. Green dotted line adjusts for Ni−Ni bond contraction upon H adsorption in the mechanical case. According to the mechanical pressure calculations, the ideal Ni−Ni bond length for HER is between 2.97 and 3.07 Å.

$Ni_3P_2(0001)$ surface of Ni_2P with $2p$ nonmetals (B, C, and O) or chalcogens at ≈50% ($n_X \approx 3$) can substantially improve the HER activity of the Ni_3-hollow site.

Dopant Substitution. Next, we evaluate the stability of different doping configurations. To do this, we calculate the free energy of substitution (ΔG_{sub}) relative to the computationally favorable phases under reducing conditions $U = 0$ V vs SHE and pH = 0 of P and each dopant (H_3PO_4, As, SiO_2, H_3BO_3, CH_4, NH_4^+, H_2O, H_2S, H_2Se, and Te)[27] for $n_X = 1$ to 6. Details and an example calculation of ΔG_{sub} for can be found in the Supporting Information (see Tables S1 and S2). Figure 1C shows that ΔG_{sub} does not depend strongly on n_X; however, a slight increase is observed for As, the chalcogens, C, N, and O. Substitution is exergonic for only five of the nine nonmetals: As, O, and the chalcogens. The others, period two nonmetals and Si, are significantly endergonic. The only set of nonmetals that both enhances the HER activity of the Ni_3-hollow site and stabilizes the surfaces is the chalcogens. O is an exception in set 2 as it substitutes spontaneously with P at $n_X = 2$ and 3. This has a negative effect on catalysis because at $n_X = 3$, where O substitution is most favorable, $\Delta G_H = 0.22$ eV, which is too weak for facile hydrogen evolution. However, since ΔG_{sub} for the heavier chalcogens are much more favorable, substitution with S, Se, and Te will be able to inhibit the introduction of O in the surface. Such substitutions can thus suppress catalytically degenerative oxygenation of the surface, highlighting another advantage of nonmetal doping. As such, we propose surface doping with S, Se, and Te as a very promising route for improving the HER activity of $Ni_3P_2(0001)$.

Exploratory Data Analysis. *Charge Descriptors.* In order to better understand the trends in ΔG_H and ΔG_{sub} with respect to n_X, we first perform a rudimentary exploratory analysis of charge descriptors. Figure 2A shows nearly linear trends between the average Ni residual charge ($\langle q_{Ni} \rangle$) and number of dopants (n_X). Their slopes can be interpreted as the direction of electron transfer between Ni and the dopant. For example, positive slopes correspond to electron transfer from Ni to the dopant, thereby oxidizing Ni (the electron donor) and reducing the nonmetal (the electron acceptor). The opposite is true for negative slopes. $\langle q_{Ni} \rangle$ does not correlate strongly with ΔG_H. For example, S and Se have very similar trends in ΔG_H (see Figure 1B). However, S and Se cause opposite shifts in $\langle q_{Ni} \rangle$. Additionally, there are no significant changes in their $\langle q_{Ni} \rangle$ trends that coincide with the maximum in ΔG_H at $n_X = 3$. Therefore, $\langle q_{Ni} \rangle$ is a poor descriptor of ΔG_H.

Important Descriptors from Machine Learning. In order to rationalize the trends in ΔG_H, we search for other structural and charge descriptors. For each DFT-relaxed structure, we compile Ni−Ni bond lengths, Ni−Ni−Ni bond angles, Löwdin charges, elemental data (mass number, atomic weight, and atomic radius), summary statistics (mean and standard deviation), and other geometric parameters (perimeter and area of Ni_3-hollow sites). Note that the descriptors we chose involve only the H adsorption site, i.e., the Ni_3-hollow site, and the dopants. Descriptors involving surface P atoms are deemed unnecessary because they do not directly participate in bonding, and changes in the Ni−P bond lengths are in fact already included in the contraction or expansion of the Ni_3-hollow sites. Removing such potentially redundant descriptors keeps the data simple. Our data are obtained from surfaces without H, because we want to be able to predict HER activity based on intrinsic surface properties. In total, the data set has 55 observations (structures) and 30 variables (29 descriptors and ΔG_H). Machine learning is becoming increasingly popular for semiautomated and quantitative discovery of data correlations in chemistry and materials science.[28−30] Using these data, we trained an RRF, yielding a root-mean-squared error (RMSE) of 0.09 eV in the predicted ΔG_H. Figure 3A shows that the data very closely straddle the perfect correlation line. Note that we performed 3-fold CV instead of randomly splitting the data into one training and one test set (see Figure S1 in the Supporting Information). In general, k-fold CV splits the data into k sets and averages the models generated by training on $k - 1$ of the sets and testing on the other. This method gives better estimates of the "out-of-sample" error, which in our case refers to the RMSE in the prediction of ΔG_H, than randomly train/test splitting.

The architecture of RRFs allows for the calculation of feature importances. These measure the relative importance of different descriptors in describing the HER activity of nonmetal-doped $Ni_2P(0001)$ surfaces. Importance is defined as the normalized ability of a descriptor to separate the data based on ΔG_H. Figure 3B shows the top ten, most important descriptors from the 29 included in our data set. The top two descriptors are a particular Ni−Ni bond length (whose constituent atoms are distinguished by their distance from the first doping site, see

DOI: 10.1021/jacs.8b00947
J. Am. Chem. Soc. 2018, 140, 4678−4683

Figure 3C) and the average Ni−Ni bond length (⟨Ni−Ni⟩). Of the top ten descriptors, seven are related to the geometry of the Ni_3-hollow site. Other important features include the charges of dopants at n_X = 2 and 3 (q_{X2} and q_{X3}), and the standard deviation of the dopant charges (σ_{qX}). While in principle, it would be straightforward to include more complex descriptors like the electronic DOS and its moments (e.g., the *d*-band center[31,32] of Ni), this is shown to be unnecessary, however, because the simple and intuitive Ni−Ni bond length proves to be quite descriptive of HER activity. Further, the fact that the atomic charges exhibit poor correlation indicates that such metrics that depend on electronic partitioning will also likely be unimportant.

Structural Descriptors. Having identified ⟨Ni−Ni⟩ as a good descriptor for ΔG_H, we more closely examine their correlation. Figure 2B shows the effect of surface doping on ⟨Ni−Ni⟩ as a function of n_X. Like ΔG_H, ⟨Ni−Ni⟩ is relatively unaffected by doping with As and Si. The period two nonmetals, however, induce a significant expansion in the ⟨Ni−Ni⟩. This correlates quite strongly (Pearson's $r \geq 0.41$, $r = -1$ or 1 for perfect negative and positive correlation, respectively) with ΔG_H, which also increases dramatically with increasing n_X. The chalcogens (set 3) show two regimes of change in ⟨Ni−Ni⟩, much like their trends for ΔG_H and ΔG_{sub}. For set 3, at lower surface doping concentrations (i.e., n_X = 1 to 3), the ⟨Ni−Ni⟩ increases with the increase for S being largest and Te the smallest. At higher surface doping concentrations (i.e., n_X = 4 to 6), ⟨Ni−Ni⟩ plateaus. While there is an apparent moderate dependence of ΔG_H or ⟨Ni−Ni⟩ on n_X seen in Figures 1B and 2B, it only became evident that Ni−Ni bond lengths are good descriptors for HER activity through the training of the RRF model. Since the influence of surface nonmetal doping on both the geometry of the Ni_3-hollow site and ΔG_H are similar, this implies a chemical pressure-like effect[33] that can be summarized as follows: nonmetal surface doping effectively acts like mechanical pressure, expanding or compressing the Ni_3-hollow site.

This effect can be rationalized as follows: as the Ni_3-hollow site expands, the Ni−H bonds that form will have to stretch if H is to remain at the center. Upon sufficient expansion, however, H must reduce/sever its interaction with one or two Ni atoms to form an optimal Ni−H bond length, thereby weakening its adsorption strength (see Figure S3 in the Supporting Information for an example of this). The HER can be broken down into two steps, H adsorption and H_2 desorption. The former is called the Volmer reaction, and its rate is proportional to the strength of H adsorption. H_2 desorption can follow either the Tafel or Heyrovsky mechanism. The rates for both of these reactions are inversely proportional to the strength of H adsorption. In order to maximize the rate of the HER, a compromise, often called the Sabatier principle,[34] must be made between H adsorption and H_2 desorption. This compromise is struck at $\Delta G_H = 0$, which is referred to as thermoneutral H adsorption. As a final comment, the Brønsted−Evans−Polanyi (BEP) principle states that there is a linear relationship between the kinetic barrier and the free energy of a reaction. Therefore, by weakening H adsorption at the Ni_3-hollow site via dopant-induced tensile strain, the kinetic barrier for HER is also decreased and its rate is increased.

Local charges play a minimal role because the surface is metallic[35] and therefore can easily provide the requisite free charge to stabilize adsorption. The effect of doping on the surface strain is nonlinear with the dopant atomic radius because the induced strain is a complex function of the relative electronegativity of the constituent atoms, valence, concentrations of the dopants, and coordination chemistry. Naturally, dopants that form shorter Ni−X bonds will expand the Ni_3-hollow site, while those that form longer Ni−X bonds will cause the Ni_3-hollow site to contract. This explains the more drastic effect of 2*p* nonmetals on the adsorption of H due to the Ni_3-hollow site's expansion. However, the mechanical effect of X on Ni−X bonding is also dependent on the dopant concentration, hence the observed nonlinear dependence of ⟨Ni−Ni⟩ on n_X (Figure 2B). These explain why the dopant atomic radius appears to be a less important descriptor for ΔG_H.

Chemical Pressure Proof of Concept. In order to confirm this machine learning insight, we apply mechanical pressure to the Ni_3-hollow site. The ⟨Ni−Ni⟩ was compressed and expanded by fixing the internal coordinates of the surface Ni atoms and allowing the other surface atoms to relax during DFT geometry optimization. Note that the lattice constants were fixed. Figure 3D shows that applied mechanical pressure (orange points and dashed line) induces the same change in ΔG_H as does chemical pressure via nonmetal doping (blue points). Therefore, it is not the electronic character of the nonmetal dopants but rather the structural distortion they induce on the surface that modulates the HER activity of the $Ni_3P_2(0001)$ surface. Note that our calculations indicate that ⟨Ni−Ni⟩ contracts by ≈0.1 Å upon H adsorption. This means that since the internal coordinates of Ni are fixed even upon H adsorption, unlike in the doping case, we are likely overestimating ΔG_H, and thus the orange line represents an upper limit for the mechanical pressure effect. If we manually adjust ⟨Ni−Ni⟩ by 0.1 Å (Figure 3D green dotted line), the agreement between mechanical and chemical pressure improves.

Perspectives. On the basis of the mechanical pressure calculations, ⟨Ni−Ni⟩ ≈ 2.97−3.07 Å should produce thermoneutral H adsorption and thus the optimal intrinsic activity for an HER electrocatalyst expressing the Ni_3 motif. The optimal bond length should be used in high-throughput searches to screen for bulk binary Ni-nonmetal compounds. An alternative would be to study mixed nonmetal doping, e.g., doping with both S and Se. We anticipate that undoped and doped transition metal phosphides with bulk crystal structures similar to $Ni_2P(s)$, such as $Fe_2P(s)$, $Co_2P(s)$, (Fe,Co)P(*s*), and (Ni,Co)P(*s*), will also exhibit chemical pressure-driven enhancement of HER to varying degrees. Our study demonstrates that a comprehensive investigation of surface nonmetal doping for a variety of single and mixed transition metal phosphides will reveal promising candidate materials with nearly ideal intrinsic activity toward the HER.

In these kinds of doping studies, we should not lose sight of the thermodynamics and kinetics of dopant incorporation and segregation within the bulk, as this will provide valuable information regarding the feasibility of synthesizing catalysts. We have shown that certain dopants may stabilize the surface with respect to dissolution, e.g., doping with chalcogens or As.

Our current data set for machine learning is specifically obtained for the Ni_2P surface that expresses the Ni_3 motif, and thus the method will work best in predicting perturbations within the structural framework of Ni_2P. A great example of extending this model would be the examination of doping with transition metals, as mentioned above, in cases where this only causes minimal changes to the underlying atomic structure of

DOI: 10.1021/jacs.8b00947
J. Am. Chem. Soc. 2018, 140, 4678−4683

Ni_2P. A model that is transferable across different bulk transition-metal phosphides would of course require additional structure-specific inputs during training. Although the RRF is trained using only a subset of dopant arrangements, having verified the predictive power of Ni_3-structure-based descriptors, the RRF model should also be able to predict the ΔG_H of other dopant configurations with high precision and accuracy.

Unlike $\langle Ni{-}Ni \rangle$, $\langle q_{Ni} \rangle$ does not correlate strongly with ΔG_H. Even though the nonmetal dopants substitute at spectator sites, it is contrary to common understanding of dopant effects that their electronic structure does not play a large role in determining HER activity. This could be explained by the fact that $Ni_2P(s)$ is metallic and therefore charge partitioning between the Ni and nonmetal components is less well-defined. This hypothesis is corroborated by the results in Figure 2A, which show that the average charge on Ni only changes by a small fraction of the charge of an electron from low to high surface doping concentrations. The structural parameters of the Ni_3-hollow site are more sensitive to changes in the surface electronic structure and therefore they are able to more accurately capture the trends between n_X and ΔG_H. This lends further support to our claim that chemical pressure is the key driving force behind the enhanced HER activity of doped $Ni_3P_2(0001)$. The connection between strain and catalytic activity has been explored in the literature, especially with regard to substrate-induced[36,37] and electrochemically induced[38] strain. For example, compressive strain was demonstrated to enhance the oxygen reduction reaction on dealloyed Pt−Cu and Pt nanoparticles via enhancement of the binding of intermediate oxygenated adsorbates,[37,38] while tensile strain was shown to stabilize CO and O chemisorption and CO dissociation on Ru(0001).[36] Here, expansion of the Ni_3 site (local, chemically induced tensile strain) reduces the affinity of H due to the reduced H coordination. The most promising catalytic system that we discovered was chalcogen-doped $Ni_3P_2(0001)$. For S (n_S = 3), the HER overpotential is −0.11 V vs SHE. This is much lower than that of the Ni_3-hollow site in the absence of dopants (−0.45 V vs SHE).[5] This overpotential is similar to that of the P-enriched, non-stoichiometric reconstruction (−0.07 V vs SHE) but this surface is only accessible upon applying −0.21 V vs SHE.[5]

SUMMARY AND CONCLUSIONS

In summary, we have demonstrated that surface nonmetal doping can significantly improve the HER activity of Ni_2P. We find that the Ni−Ni bond length is an effective descriptor for the HER activity of $Ni_3P_2(0001)$ of Ni_2P and hence can be used in a computationally efficient, high-throughput search to screen for promising Ni-nonmetal catalytic materials. We have shown how machine learning methodologies can be implemented in the catalyst design pipeline to automatically discover and rank the importance of structural and charge-based descriptors for HER. Machine learning is highly customizable in that many different model types can be selected (here we choose RRFs) and the number and types of descriptors is limited only by scientific creativity. We validated the results from our machine learning by applying mechanical pressure to compress and expand the Ni_3-hollow sites, which showed that the effects of chemical pressure via nonmetal doping and mechanical pressure are in excellent agreement. Our results strongly indicate that it is the induced local geometry of the Ni_3-hollow site and not the electronic character of the dopants that improves the HER activity of $Ni_3P_2(0001)$. We believe that this insight should spur both experimental and theoretical research in surface nonmetal doping of transition metal phosphides in the wider effort find ideal HER catalysts.

ASSOCIATED CONTENT

Supporting Information

The Supporting Information is available free of charge on the ACS Publications website at DOI: 10.1021/jacs.8b00947.

Additional computational details, additional theoretical details, tabulated standard oxidation/reduction free energy of nonmetal standard states to form most stable phases, tabulated free energy of substituting P with other nonmetals relative to their standard states, the relative importance of all descriptors calculated from the RRF model, and sample illustrations of the effect of Ni_3-hollow site expansion induced by doping with nonmetals on the strength of Ni−H bonds (PDF)

Machine learning data (ZIP)

Structure data (ZIP)

AUTHOR INFORMATION

Corresponding Author

*rappe@sas.upenn.edu

ORCID

Robert B. Wexler: 0000-0002-6861-6421

John Mark P. Martirez: 0000-0003-0566-6605

Andrew M. Rappe: 0000-0003-4620-6496

Notes

The authors declare no competing financial interest.

ACKNOWLEDGMENTS

R.B.W., J.M.P.M., and A.M.R. acknowledge support from the Office of Naval Research under grant number N00014-17-1-2574. The authors also acknowledge computational support from the High-Performance Computing Modernization Office and the National Energy Research Scientific Computing Center.

REFERENCES

(1) Hinnemann, B.; Moses, P. G.; Bonde, J.; Jørgensen, K. P.; Nielsen, J. H.; Horch, S.; Chorkendorff, I.; Nørskov, J. K. *J. Am. Chem. Soc.* **2005**, *127*, 5308−5309.

(2) Jaramillo, T. F.; Jørgensen, K. P.; Bonde, J.; Nielsen, J. H.; Horch, S.; Chorkendorff, I. *Science* **2007**, *317*, 100−102.

(3) Liu, P.; Rodriguez, J. A. *J. Am. Chem. Soc.* **2005**, *127*, 14871−14878.

(4) Popczun, E. J.; McKone, J. R.; Read, C. G.; Biacchi, A. J.; Wiltrout, A. M.; Lewis, N. S.; Schaak, R. E. *J. Am. Chem. Soc.* **2013**, *135*, 9267−9270.

(5) Wexler, R. B.; Martirez, J. M. P.; Rappe, A. M. *ACS Catal.* **2017**, *7*, 7718−7725.

(6) Liang, H.; Gandi, A. N.; Anjum, D. H.; Wang, X.; Schwingenschlögl, U.; Alshareef, H. N. *Nano Lett.* **2016**, *16*, 7718−7725.

(7) Feng, Y.; Yu, X.-Y.; Paik, U. *Chem. Commun.* **2016**, *52*, 1633−1636.

(8) Li, J.; Yan, M.; Zhou, X.; Huang, Z.-Q.; Xia, Z.; Chang, C.-R.; Ma, Y.; Qu, Y. *Adv. Funct. Mater.* **2016**, *26*, 6785−6796.

(9) Wang, P.; Pu, Z.; Li, Y.; Wu, L.; Tu, Z.; Jiang, M.; Kou, Z.; Amiinu, I. S.; Mu, S. *ACS Appl. Mater. Interfaces* **2017**, *9*, 26001−26007.

(10) Zhang, Y.; Liu, Y.; Ma, M.; Ren, X.; Liu, Z.; Du, G.; Asiri, A. M.; Sun, X. *Chem. Commun.* **2017**, *53*, 11048−11051.

DOI: 10.1021/jacs.8b00947
J. Am. Chem. Soc. 2018, 140, 4678−4683

(11) Sun, Y.; Hang, L.; Shen, Q.; Zhang, T.; Li, H.; Zhang, X.; Lyu, X.; Li, Y. *Nanoscale* **2017**, *9*, 16674−16679.
(12) Shalom, M.; Ressnig, D.; Yang, X.; Clavel, G.; Fellinger, T. P.; Antonietti, M. *J. Mater. Chem. A* **2015**, *3*, 8171−8177.
(13) Swesi, A. T.; Masud, J.; Nath, M. *Energy Environ. Sci.* **2016**, *9*, 1771−1782.
(14) Yang, W.; Rehman, S.; Chu, X.; Hou, Y.; Gao, S. *ChemNanoMat* **2015**, *1*, 376−398.
(15) Deng, H.; Runger, G. *Pattern Recognit.* **2013**, *46*, 3483−3489.
(16) Giannozzi, P.; Baroni, S.; Bonini, N.; Calandra, M.; Car, R.; Cavazzoni, C.; Ceresoli, D.; Chiarotti, G. L.; Cococcioni, M.; Dabo, I.; Corso, A. D.; de Gironcoli, S.; Fabris, S.; Fratesi, G.; Gebauer, R.; Gerstmann, U.; Gougoussis, C.; Kokalj, A.; Lazzeri, M.; Martin-Samos, L.; Marzari, N.; Mauri, F.; Mazzarello, R.; Paolini, S.; Pasquarello, A.; Paulatto, L.; Sbraccia, C.; Scandolo, S.; Sclauzero, G.; Seitsonen, A. P.; Smogunov, A.; Umari, P.; Wentzcovitch, R. M. *J. Phys.: Condens. Matter* **2009**, *21*, 395502.
(17) Rappe, A. M.; Rabe, K. M.; Kaxiras, E.; Joannopoulos, J. D. *Phys. Rev. B: Condens. Matter Mater. Phys.* **1990**, *41*, 1227−1230.
(18) Ramer, N. J.; Rappe, A. M. *Phys. Rev. B: Condens. Matter Mater. Phys.* **1999**, *59*, 12471−12478.
(19) Perdew, J. P.; Burke, K.; Ernzerhof, M. *Phys. Rev. Lett.* **1996**, *77*, 3865.
(20) Grimme, S. *J. Comput. Chem.* **2006**, *27*, 1787−1799.
(21) Barone, V.; Casarin, M.; Forrer, D.; Pavone, M.; Sambi, M.; Vittadini, A. *J. Comput. Chem.* **2009**, *30*, 934−939.
(22) Ramalho, J. P. P.; Gomes, J. R.; Illas, F. *RSC Adv.* **2013**, *3*, 13085−13100.
(23) Eder, F.; Lercher, J. A. *Zeolites* **1997**, *18*, 75−81.
(24) Zhou, Z.; Zhao, J.; Chen, Z.; Gao, X.; Yan, T.; Wen, B.; Schleyer, P. v. R. *J. Phys. Chem. B* **2006**, *110*, 13363−13369.
(25) Krishnan, S.; Vadapoo, R.; Riley, K. E.; Velev, J. P. *Phys. Rev. B: Condens. Matter Mater. Phys.* **2011**, *84*, 165408.
(26) Kuhn, M. *J. Stat. Softw.* **2008**, *28*, 1−26.
(27) Jain, A.; Ong, S. P.; Hautier, G.; Chen, W.; Richards, W. D.; Dacek, S.; Cholia, S.; Gunter, D.; Skinner, D.; Ceder, G.; Persson, K. a. *APL Mater.* **2013**, *1*, 011002.
(28) Saal, J. E.; Kirklin, S.; Aykol, M.; Meredig, B.; Wolverton, C. *JOM* **2013**, *65*, 1501−1509.
(29) Ivanciuc, O. *Reviews in Computational Chemistry* **2007**, *23*, 291−400.
(30) Handley, C. M.; Popelier, P. L. *J. Phys. Chem. A* **2010**, *114*, 3371−3383.
(31) Nørskov, J. *Prog. Surf. Sci.* **1991**, *38*, 103−144.
(32) Hammer, B.; Norskov, J. *Nature* **1995**, *376*, 238−240.
(33) Raaen, S.; Parks, R. *Solid State Commun.* **1983**, *48*, 199−202.
(34) Sabatier, P. *La Catalyse en Chimie Organique*; Berague: Paris, France, 1920.
(35) Wexler, R. B.; Martirez, J. M. P.; Rappe, A. M. *Chem. Mater.* **2016**, *28*, 5365−5372.
(36) Mavrikakis, M.; Hammer, B.; Nørskov, J. K. *Phys. Rev. Lett.* **1998**, *81*, 2819−22.
(37) Strasser, P.; Koh, S.; Anniyev, T.; Greeley, J.; More, K.; Yu, C.; Liu, Z.; Kaya, S.; Nordlund, D.; Ogasawara, H. *Nat. Chem.* **2010**, *2*, 454−460.
(38) Wang, H.; Xu, S.; Tsai, C.; Li, Y.; Liu, C.; Zhao, J.; Liu, Y.; Yuan, H.; Abild-Pedersen, F.; Prinz, F. B. *Science* **2016**, *354*, 1031−1036.

DOI: 10.1021/jacs.8b00947
J. Am. Chem. Soc. 2018, 140, 4678−4683